Hollow Metal Nanorods with Tunable Dimensions, Porosity, and Photonic Properties

Nathanael R. Sieb, Nien-chen Wu, Elham Majidi, Richa Kukreja, Neil R. Branda, and Byron D. Gates*

4D LABS, Department of Chemistry, Simon Fraser University, 8888 University Drive, Burnaby, BC V5A 1S6 Canada

ARTICLE

ABSTRACT An important aspect of synthesizing designer nanostructures is fine-tuning their size, composition, and surface area. These parameters often dictate the unique properties of nanoparticles relative to their bulk counterpart. This paper reports the synthesis of porous metal nanorods with well-controlled dimensions, porosity, and photonic properties. The growth of each nanostructure is directed by a polycrystalline sacrificial template of silver with well-defined, tunable dimensions. This template can be selectively etched to isolate a porous hollow nanostructure. The porosity, composition, and photonic characteristics of this nanostructure are adjustable by controlling the reaction conditions.

KEYWORDS: porous nanorods · hollow nanostructures · electrodeposition · galvanic replacement · template directed synthesis · polycrystalline silver nanorods · surface plasmon resonance

A versatile method to prepare porous hollow nanoparticles with tunable dimensions, porosity, and photonic properties would offer a modular route to structures that have potential use in numerous applications. One example is in the area of photodynamic therapy, where the use of nanoparticles as drug-delivery vehicles relies on their having the appropriate size and shape for efficient endocytosis as well as their photonic properties for their optical response.[1−4] Optical markers and biological tracers would also benefit from the unique photonic properties imparted from the small size and large surface area of nanoparticles.[5−11]

We have developed an adaptable approach for preparing materials of engineered size, shape, composition, and porosity. A scalable approach to the synthesis of these materials is through solution-phase synthesis of nanostructures that are templates for the further growth of an exterior shell that can serve as the precursor to the desired hollow structure. Through selective removal of the core template,[12−14] a hollow structure can be isolated. Tuning the composition and porosity of these materials is not as straightforward as tuning the size and shape, which depend on the same features within the original template. Unlike previous demonstrations of the synthesis of porous hollow nanorods,[15,16] we opted to use a polycrystalline nanorod[17−20] as the sacrificial template to direct the growth of the exterior shell. The consequence of there being multiple reactive sites along the polycrystalline nanorod is that reactions take place simultaneously along the length of the template. This increase in reactive sites relative to previous demonstrations in the literature leads to a fine control over the final porosity and composition of the isolated hollow nanorod as demonstrated herein. We further demonstrate the versatility of our method by tuning the length, diameter, and photonic properties of the isolated hollow nanostructures.

Two prerequisites are necessary to take full advantage of porosity as a parameter to develop an adaptable approach to prepare materials with tunable surface area and photonic properties. One is a nanoscale template with controlled morphology, composition, and dimensions. The other is a convenient, scalable synthetic technique capable of transferring the topological information programmed into the template to that of a final structure. Our method addresses both requirements by taking advantage of the beneficial features of two synthetic strategies. (1) The templates are grown using electrochemical deposition, which is ideal for controlling reaction rates and localizing the template growth to a confined volume. (2) Galvanic replacement is an efficient and tunable process for the formation of hollow nanostructures of desired dimensions and porosity. Because the galvanic Ag → Au replacement reaction proceeds from the exterior to the

*Address correspondence to bgates@sfu.ca.

Received for review January 31, 2009 and accepted May 06, 2009.

Published online May 13, 2009.
10.1021/nn900099t CCC: $40.75

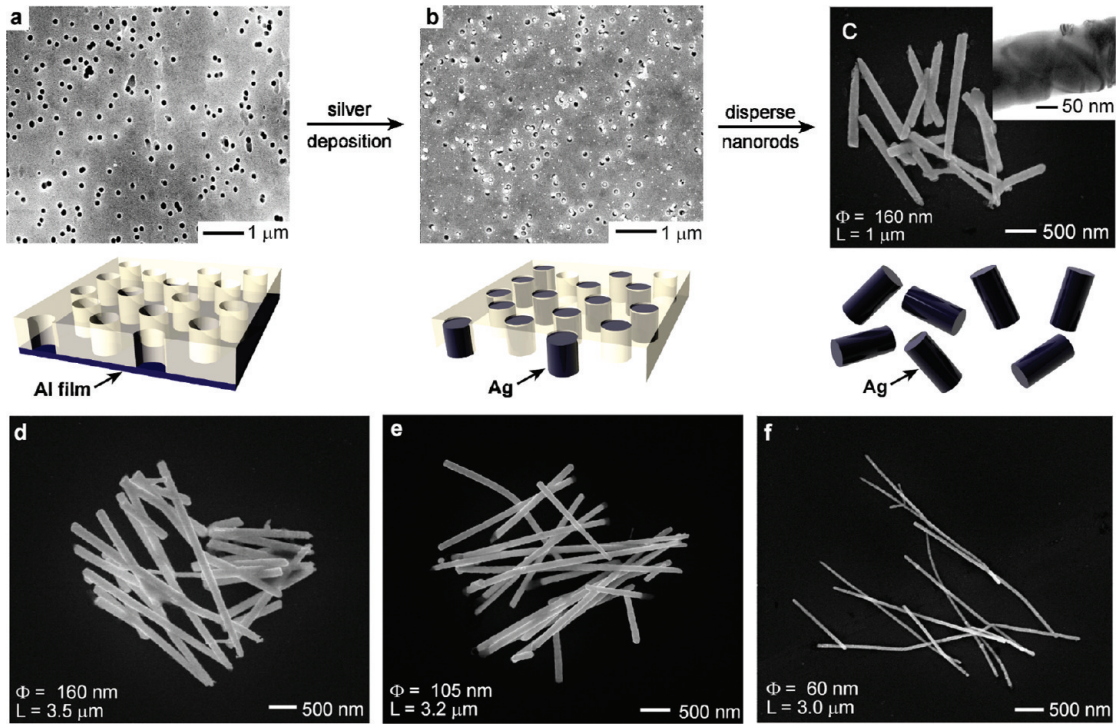

Figure 1. Scanning electron microscopy (SEM) images and schematic representations of (a) the polycarbonate substrate containing one-dimensional, vertical pores that serve as physical molds for the growth of silver nanostructures, (b) the pores after electrodeposition of silver within them, (c) the isolated silver nanostructures after dissolving the aluminum electrode film and the polymer substrate, and (d−f) silver nanorods with diameters of 160, 105, and 60 nm and lengths ranging from 1.5 to 3.5 μm (Φ = average diameter and *L* = average length). The inset in (c) contains a transmission electron microscopy (TEM) image that shows the polycrystalline nature of these silver nanorods.

interior of the template, it can be stopped at any point, the remaining silver template can be selectively etched, and a hollow structure with controlled porosity can be isolated. Fine-tuning the final porosity is possible because it is a direct function of the amount of gold deposited onto the template before etching.

RESULTS AND DISCUSSION

The growth of uniform cylindrical templates is illustrated in Figure 1. A high level of control over dimensionality is achieved by confining the solution-phase electrochemical deposition of the silver to the inside of the vertical channels (~6 μm in length, 10−100 nm in diameter) provided by commercially available Sterlitech track-etched polycarbonate (Figure 1a). The growth is directed by capping one end of the channels by thermally evaporating a 200 nm thick aluminum film onto one side of the polycarbonate, which also acts as the working electrode during the electrodeposition of silver into the pores of the polycarbonate substrate. The electrodeposition is carried out by filling the open channels with an electrolyte solution containing a silver salt (in the present case, AgCN) and applying an appropriate voltage. Prior to electrodeposition, the channels must be exposed to oxygen-based plasma to reduce their hydrophobic nature. Without this pretreatment, pockets of air readily trap within the channels, which would decrease the yield of electrochemically grown silver nanostructures. The two-fold increase in the number of channels containing silver nanostructures produced when the electrochemical reaction is carried out within the hydrophilic channels supports the need for this plasma treatment.[21] Alternatively, the pores of the membranes can be modified with Sn^{2+}, as described in the Methods, to maximize the yield of nanorods (Figure 1b). On the basis of the manufacturer supplied pore density of 6×10^8 pores/cm^2 and a deposition area of ~3.46 cm^2, we estimate that each electrodeposition process yields $\sim 2.1 \times 10^9$ silver nanorods. Larger sample sizes can be achieved by combining the nanorods from multiple processes. The filled channels are observed after selectively removing the aluminum electrode by wet chemical etching with an aqueous base (KOH) and imaging the resulting film by SEM.

The growth of the silver templates is controlled by regulating the voltage applied to the channels during the electrochemical reduction of the silver cation within the physical molds. The dimensions of the final structures can be confirmed by imaging them (Figure 1d−f) after selectively removing both the aluminum electrode (with aqueous KOH) and polycarbonate mold (with $CHCl_3$) and purifying them by repeated centrifugation and washing steps (see Methods for the purification procedure). Although the electrodeposition will proceed as long as the applied potential is sufficient to reduce Ag^+ to Ag^0 at the growing electrode surface, the

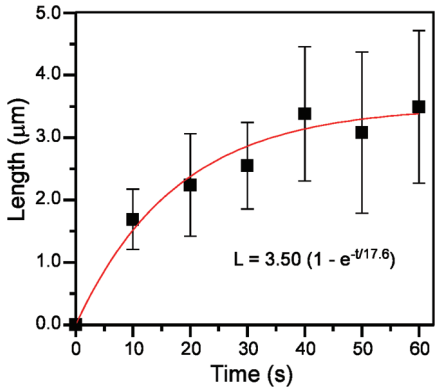

Figure 2. Dependence of silver nanorod length (*L*) on the duration of electrodeposition (*t*). Data for this plot were collected for 160 nm diameter silver nanorods electrodeposited into the pores of a polycarbonate membrane. Error bars are plotted to represent one standard deviation from a population of at least 25 nanorods.

rate of metal deposition and delivery of reactants to the electrode must be moderated by adjusting the applied potential. The optimal difference in potential is approximately 1.75 V relative to a Ag/AgCl reference electrode, which fills the channels in the polycarbonate substrate with silver at an average vertical growth rate of ~75 nm s^{-1} (Figure 2). Larger differences in potential (≥2.00 V) result in electrodeposition at a rate that is too high to control the dimensions of the nanostructures, and upon filling the channels, excess silver continues to deposit and eventually covers the polycarbonate substrate with large irregular aggregates of metal.[22] At the lower difference in potential (1.75 V), cylindrical anisotropic nanoparticles (nanorods) can be grown with lengths up to 3.5 μm by regulating the duration of the electrochemical reaction.

We anticipated that the length of the isolated nanorods would consistently increase with the length of electrodeposition. However, observations of the average length of nanorods obtained after reaction times up to 60 s at 1.75 V indicate the trend deviates from linearity (Figure 2). The growth rate of the silver nanorods decays exponentially from 180 to ~20 nm s^{-1} as the length of the nanorods increases. This apparent decrease in growth rate might be the result of fragility of these high aspect ratio nanostructures, especially those approaching lengths of 6 μm.[23] nanorods of a diverse range of lengths are present in Figure 1d. These structures could break into shorter fragments from the repeated cycles of centrifugation during the purification process. This fragmentation could account for the larger deviation in particle lengths observed for longer periods of electrodeposition.

Nanostructures grown within the cylindrical pores of each track-etched polycarbonate substrate mimic the shape and dimensions of the channels that confine their growth, albeit they are ~55 nm larger (60, 105, and 160 nm) than the diameters reported for the channels in the substrate (10, 50, and 100 nm). Care must be taken when relying on the reported dimensions of the polycarbonate substrate as they are often measured using SEM techniques to image only the exterior opening of the channel, which is inconsistent with the actual diameter of the channel within the substrate. Our findings on the mismatch between these two dimensions are consistent with other reports.[23,24] The silver nanorods grown by our method have aspect ratios between ~20 and 150, which show the heightened control over the final dimensions as compared to solution-phase synthesis.[25−28]

Another difference between silver nanorods grown by solution-phase synthesis and our electrochemical deposition is the crystallinity of the products. Silver nanorods grown by our electrodeposition technique are polycrystalline. Multiple crystal boundaries with irregular orientations are observed along each nanorod when observed by TEM (Figure 1c inset). nanorods of silver grown by solution-phase techniques are, however, composed of pentagonally twinned crystalline lattices, each extending the length of the nanorod.[26] These regular crystalline lattices of silver were used for the first demonstrations of galvanic replacement reactions on anisotropic silver nanostructures.[15,16] It is our expectation that polycrystalline nanorods of silver will react faster and more uniformly along the length of the nanorod during the galvanic displacement reaction. This prediction is partially based on the reactivity of atoms at the boundaries between each crystalline facet.[29,30] A nanorod of polycrystalline silver offers multiple reactive sites along the length of the nanostructure. Another impediment for a uniform galvanic displacement reaction on the pentagonally twinned crystalline lattices is the preference of surfactants to bind to the {100} facets, which run the length of these nanorods.[26,28] Therefore, the surfaces preferentially exposed during galvanic replacement are the {111} facets located at each end of the these anisotropic nanostructures. Multiple facets exposed along the length of our silver nanorods grown by electrodeposition should improve the uniformity and speed of the galvanic displacement process along the length of the nanorod.

The dimensionality of the nanorod template can be translated to the final nanostructure with a high level of control. The exposed surfaces of the silver template are sacrificed (oxidized to soluble silver salts) by galvanic replacement during growth of the gold or alloy-based nanostructures (Figure 3). During the initial stages of the exchange reaction, the surface of the silver nanorod is decorated with gold nanoparticles (Figure 3a). As the reaction proceeds, the silver template is coated with an increasingly dense shell of gold metal. We selectively etch the remaining silver template in the presence of ammonium hydroxide. This process removes the silver core of the nanorod template as well as any silver chloride precipitate remaining from the galvanic replacement reaction. After this etching process, the isolated metal struc-

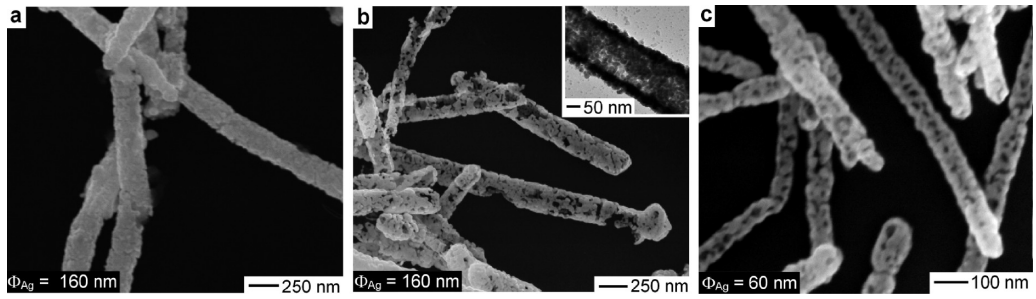

Figure 3. (a−c) These SEM images are of nanostructures prepared by galvanic replacement reactions of silver nanorod templates. The process begins with (a) the deposition of gold nanoparticles onto the surface of 160 nm diameter silver templates, followed by (b) selective etching of the remaining silver core with ammonium hydroxide to produce hollow structures of a gold−silver alloy (the inset shows a TEM image of a single hollow nanorod). This process can also be extended to (c) templates of 60 nm diameter silver nanorods.

tures are hollow, porous nanostructures (Figure 3b). The hollow nanostructures have dimensions larger than those of the silver templates. A possible contribution to this increase in dimensions is that the galvanic reaction proceeds through a surface dominated reaction. Gold atoms initially deposit onto the surface of the silver nanorod templates and form either particles of gold or Au−Ag. The increase in dimensions is measurable. For example, a 60 nm diameter silver nanorod template produces 80 nm diameter hollow nanorods following the galvanic replacement process (Figure 3c). Our metal nanostructures synthesized by galvanic replacement and selective etching are mechanically stable. Polyvinylpyrrolidone (PVP) used to disperse the silver templates following removal of the polycarbonate substrate can also be used to disperse the porous hollow nanostructures. This surfactant prevents these metal nanostructures from irreversibly aggregating (cold welding). The purification procedure involves repeated centrifugation steps and subsequent dispersion in the rinse solvent by vortexing or otherwise vigorously shaking the sample. The porous hollow nanostructures remain intact following this purification process.

The mechanism of galvanic replacement for our polycrystalline silver nanorods is different from that for the pentagonally twinned nanorods with regular crystalline lattices of a five-fold symmetry. We synthesized silver nanorods with a pentagonally twinned lattice by a solution-phase technique[28] to compare the reactivity of this template with the nanorods grown by electrodeposition. Galvanic replacement on the twinned crystalline lattices initiates at only a few sites randomly along the nanorod (Figure 4) in contrast to the polycrystalline nanorods with multiple sites of gold deposition distributed over the length of the nanorod. This difference is observed in the nonuniform porosity along the twinned crystalline lattice of silver during galvanic replacement as well as the lack of structural uniformity after isolation of the hollow nanorod. Extension of this replacement process to silver nanorods with randomly oriented crystalline domains along the length of the template increases the number of reactive sites. The increased reactivity along the silver template strengthens the shell of the isolated hollow nanorod following etching of the remaining silver with ammonium hydroxide. The different mechanism of reactivity between our nanorods and the pentagonally twinned nanorods could lead to more than a structural difference in the product. This distinction also produces nanostructures with a noticeable difference in porosity. Our approach leads to a hollow nanorod with a wider range of synthetically accessible porosities.

Our method for the synthesis of porous hollow nanostructures produces particles with a controlled composition and porosity. Figure 5a summarizes our approach to controlling these parameters. Control is achieved through regulating conditions of the galvanic replacement reaction, such as the concentration of gold salt. Elemental analysis by energy dispersion X-ray spectroscopy (EDS) confirms the composition of the particles during each stage of the galvanic replacement reaction (Figure 5b). These measurements indicate a decrease in silver content with progressively increasing concentrations of gold salt used during the replacement reaction. Electron microscopy analysis provides further insight into the different stages of the reaction. The morphology of the hollow metal nanostructures is tuned by controlling the dimensions of the silver template and the conditions of the galvanic replacement process. The silver nanorod templates can be converted into hollow metal nanostructures with controlled porosity (Figures 4d−f and 5c−e). Analysis by EDS and X-ray photoelectron spectroscopy (XPS) has identified that these hollow nanostructures contain both gold and silver. Etching the silver core with NH_4OH does not remove the silver from this alloy, which is different from the results reported previously by Murphy.[14] The silver−gold alloy increases the stability of the hollow structure isolated at early stages of the galvanic replacement reaction.

In order to confirm the presence of a gold−silver alloy in the porous nanorods, several samples were analyzed by XPS.[32] In a nanorod containing 80% gold and 20% silver, the positions of the Ag 3d doublet are 368.08 and 374.10 eV and the Au 4f doublet are 84.18 and 87.85 eV. These peak positions match the XPS re-

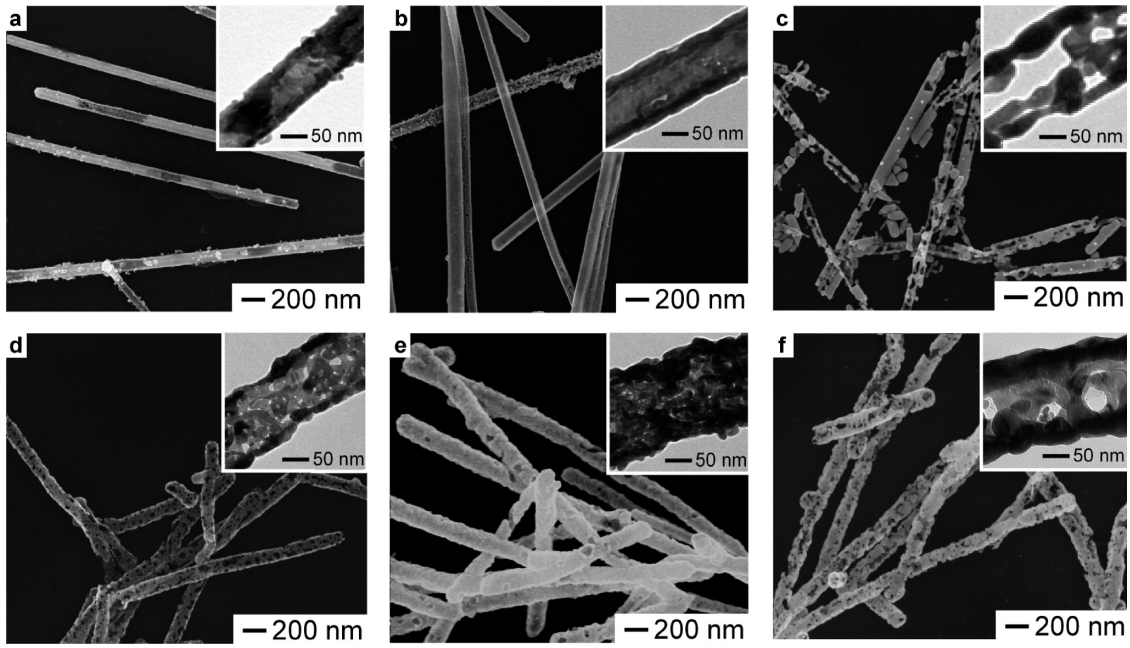

Figure 4. These SEM images show the different morphologies of porous nanorods when the templates are pentagonally twinned nanorods (a−c) *vs* our polycrystalline nanorods (d−f). The insets contain high-magnification TEM images to emphasize the differences in porosity and structural uniformity of the hollow nanorods. All of the nanorods in these images have been treated with ammonium hydroxide to etch away the excess silver following the galvanic replacement process.[31]

sults for a gold−silver alloy in ref 33. In addition, the binding energy of gold shifts toward that of pure gold (84.0 and 87.7 eV) as the gold content of the nanorods increased from 0 to 86%. This shift can be attributed to a loss of silver in the alloy. Conversely, the binding energy of silver shifts further from that of pure silver (368.4 and 374.4 eV) with an increasing concentration of gold. This XPS analysis confirms the formation of an alloy and the concentration of gold and silver in each of the porous, hollow nanorods. In addition, compositions of the nanorods in Figure 5c−e were determined to be $Au_{0.31}Ag_{0.69}$, $Au_{0.71}Ag_{0.29}$, and $Au_{0.86}Ag_{0.14}$, respectively.

The porosity of the hollow nanostructures is tuned by varying the amount of added gold salt (Figure 5c−e). Increasing the concentration of Au^{3+} from 0.02 to 0.14 mM leads to a significant decrease in both the

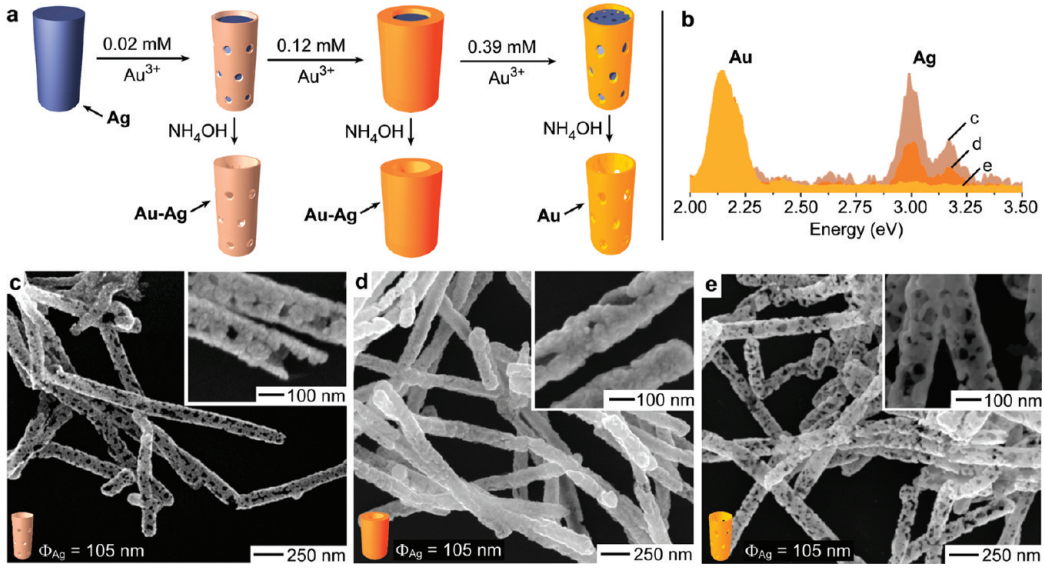

Figure 5. (a) Summary of the galvanic replacement process illustrating how the silver templates are converted into porous hollow nanostructures of gold or a gold−silver alloy. The open ends of the cartoons are not meant to imply the structures are not capped on the end with metal, but are simply used to reveal the interior of each structure. (b) EDS data for the hollow metal nanostructures shown in (c−e) indicate a decreased silver content with increasing gold salt concentration. (c−e) SEM images of porous hollow nanorods prepared by galvanic replacement and selective etching. Increasing the total concentration of gold salt (c) 0.02 mM, (d) 0.14 mM, (e) 0.53 mM varies the porosity and composition of the isolated nanostructure from (c) a porous gold−silver alloy to (d) a hollow gold−silver alloy to (e) a porous structure of predominately gold.

dimensions and density of the pores within the hollow nanostructures, and a more complete shell of gold and silver surrounds the template as is clearly seen by comparing the SEM images in Figure 5c,d. Pore size in these two products decreases from an average of ~50 to ~30 nm along with a large decrease in pore density from 4.8 ± 0.6 pores/100 nm for the sample in Figure 5c to 0.52 ± 0.16 pores/100 nm for the sample in Figure 5d. These pore densities were obtained by counting pores within the nanorods as observed in the SEM images. More accurate methods for measuring porosity could not be implemented due to the small quantity of product from each synthesis. Further increasing the total gold concentration to 0.53 mM removes more of the silver from the template and begins to remove silver from the shell of Au−Ag alloy, leaving a thin shell of predominately gold over the silver core. The pore size of the isolated structures increases from ~30 to ~70 nm along with an increase in the pore density to 4.2 ± 0.6 pores/100 nm. The isolated structures are porous hollow nanostructures of predominately gold (Figure 5e). Reaction time, or length of exposure to the gold salt, could be varied to further control the porosity and composition of the isolated metal nanostructures.

Changes in composition and porosity will alter the photonic properties of the hollow nanorods. UV−vis spectra were measured for individual silver templates and porous, hollow nanorods. Comparisons were carried out for the transverse plasmon band. The longitudinal plasmon band is >1000 nm, which is beyond the range of our spectrometer. The peak intensity of the scattered light collected from the hollow nanostructures of a gold−silver alloy and gold is red-shifted when compared to the original polycrystalline silver nanorod (Figure 6). The observed spectral red shift is consistent with a change in composition from a silver nanorod[15,34] to a gold nanorod.[34,35] The shoulder of the spectral peaks for our hollow nanorods is consistent with previously reported observations for hollow nanocubes. These spectral features were, however, not observed for hollow nanotubes of alloyed Au−Ag synthesized from templates of pentagonally twinned silver nanorods.[15] This result suggests that the shoulder within our spectral measurements corresponds to the porosity and morphology of our hollow nanorods. Further spectral shifts may be monitored for analytes binding to and releasing from the surface of these hollow nanostructures.[36,37] The tunable porosity of our product would increase the accessible surface area of the metal nanostructure for detecting analytes, as well as decreasing the response time of the material to changes in analyte concentration within a solution.

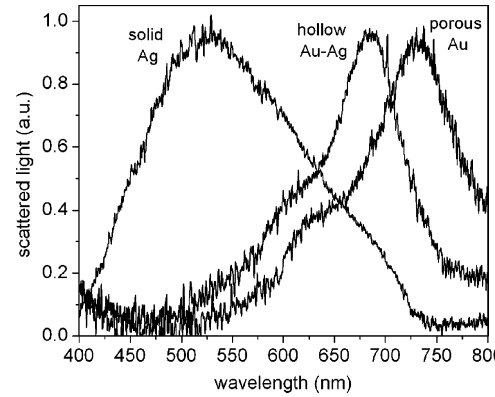

Figure 6. Scattered light from the nanorods red shifts from 530 nm for the solid silver nanorods, to 690 nm for a hollow nanorod with a complete gold−silver shell ($Au_{0.71}Ag_{0.29}$), to 740 nm for a porous hollow nanorod of predominately gold ($Au_{0.86}Ag_{0.14}$). These are average spectra for single nanorods with a diameter of 140 nm and a length of ~2 μm.

CONCLUSIONS

We have developed a simple technique to engineer hollow metal nanostructures of well-defined porosity, dimensions, and photonic properties. These nanostructures have a tunable diameter, length, and shape that are defined by the sacrificial template used to grow the hollow product. The electrochemically synthesized templates are regular, polycrystalline cylindrical silver nanorods with dimensions dictated by both the physical mold that confines their growth as well as the conditions for electrodeposition. The silver template particles are conveniently converted into hollow metal nanostructures using a galvanic replacement reaction, which offers a versatile approach to produce robust hollow nanostructures with tunable compositions, photonic properties, and porosity (both density and dimensions of the pores can be modified). These robust hollow metal nanostructures have potential applications in the selective delivery and release of reagents such as medicinal drugs. Both the porosity (as demonstrated in this report) and the surface chemistry[5,38−41] of these metal nanostructures can be simultaneously controlled for these and other applications. A complementary application is the use of the tunable photothermal properties of these nanostructures that depend on the nanoscale dimensions and composition of the nanostructure. The photothermal properties of metal nanostructures have been investigated for destroying cancer cells.[1,16,42,43] We will assess the suitability of our tunable hollow metal nanostructures for these applications in future studies.

METHODS

Setup for Electrodeposition of Silver. Polycarbonate substrates (~6 μm thick and 25 mm in diameter, Sterlitech Inc.) were exposed to O_2 plasma at 0.4 Torr for 30 s using a Harrick Scientific plasma cleaner. These polycarbonate membranes were immersed into a solution of 26 mM $SnCl_2$ and 70 mM trifluoroacetic acid in 50% (v/v) methanol/water for 5 min and subsequently rinsed with methanol and dried under a stream of N_2(g).[44] One side of each substrate was

coated with a 200 nm thick film of aluminum (99.99%, Strem Chemicals) by thermal evaporation (CHA Industries, Model #SE-600-RAP, base pressure of $<2 \times 10^{-6}$ Torr) at a deposition rate of approximately 1 nm s^{-1}. The discs were placed aluminum side down on the top of an aluminum plate, which was pretreated with a few drops of a saturated NaCl solution to serve as a conductive layer between the two aluminum surfaces. A glass tube containing a Ag/AgCl wire in a saturated aqueous solution of silver chloride was used as the reference electrode, and a Pt wire (~99.95%, Strem Chemicals) inserted into a glass tube containing a glass frit and filled with the electroplating solution was used as the counter electrode (see Figure S1 in Supporting Information). The electrodeposition setup included a bipotentiostat (Model AFCBP) from Pine Research Instrumentation controlled using PineChem 2.5 software.

Synthesis of Silver nanorod Templates. The nanorod templates were synthesized by electrodepositing silver into the pores of the polycarbonate substrate from a silver plating solution (Transene Co.) containing 2.6−4.6% (w/v) AgCN. The silver electroplating solution was mixed with a stream of nitrogen gas bubbles, which were delivered *via* a glass pipet into the solution just above the polycarbonate substrate at a nitrogen delivery rate of ~0.5 mL s^{-1}. A difference in potential of 1.75 V between the working and counter electrode was applied for 10−60 s depending on the desired length of the silver nanostructure. The growth reaction was monitored by plotting the current as a function of time using the PineChem software. After the appropriate length of time, the polycarbonate substrate was rinsed with more than 10 mL of 18.2 MΩ water and immersed in an aqueous solution of 30% (w/v) KOH (EMD Inc.) for 30 s to remove the aluminum film. The substrate was washed with 18.2 MΩ water and dried under a flow of nitrogen gas. The silver nanostructures were isolated by dissolving the polycarbonate in ~5 mL of $CHCl_3$ (99.8%, Caledon Inc.) for 5 min. The isolated silver nanostructures were purified to remove the polycarbonate by concentrating these nanostructures under centrifugation (2000 rpm, 2 min), decanting the supernatant, and redispersing the nanostructures in a solution of 0.4% (w/v) polyvinylpyrrolidone (PVP) in 99.5% EtOH (Aldrich). The centrifuging−decanting−redispersing process was repeated three times and mixed in the final wash solution for 3 h. The nanostructures were further purified by subjecting them to three washing cycles as described above but replacing the EtOH solution with a solution of 0.4% (w/v) PVP in 18.2 MΩ water. Samples were stable for >6 months when stored in a 5 mL solution of 0.4% PVP in high purity water.

Synthesis of Porous Hollow nanostructures. The hollow metal nanostructures were prepared by galvanic replacement of the silver in the nanorod template using an aqueous solution of 1 mM chloroauric acid, which was prepared by dissolving hydrogen tertracholoroaurate trihydrate (99.99%, Sigma-Aldrich) in water and allowing this solution to stand for more than 24 h prior to use to permit complete dissolution of the gold salt under ambient conditions. The galvanic replacement process was initiated by heating a 10 mL aqueous suspension of the silver templates (~4.2×10^9 nanorods) and 0.4% PVP at reflux for 10 min in a round-bottom flask and treating it with the solution of gold salt in necessary quantities to achieve a final concentration of 0.02−0.7 mM chloroauric acid (*e.g.*, add 0.2 mL of 1 mM chloroauric acid to achieve a final concentration of 0.02 mM). After mixing for at least 1 min, the reaction was cooled and the nanostructures were purified by three cycles of centrifuging (1000 rpm, 2 min), decanting, and resuspending them in high purity water. The gold or gold−silver alloy nanostructures were isolated by selectively etching any remaining silver core by dispersing them in 0.5 mL of ammonium hydroxide (~30% in water, w/w, EMD Inc.) for at least 30 min. No further change or distinguishable degradation of the porous nanostructures was observed after dispersion in a solution of ammonium hydroxide for up to 2 days. These porous nanostructures were purified by the same method of centrifuging−decanting−redispersing as used for the silver templates. The same procedure was used regardless of the dimensions of the silver nanorod templates. A variety of chloroauric acid concentrations (*e.g.*, 0.02, 0.14, and 0.53 mM) are used to obtain a variety of morphologies. Characterization of these structures was performed by SEM, TEM, EDS, XPS, and UV−vis spectral analysis.

Characterization. The nanostructures were characterized by scanning electron microscopy (SEM; FEI Strata 235DB FESEM/FIB, 10 kV) and transmission electron microscopy (TEM; FEI Tecnai G2 STEM, 200 kV) each equipped with energy dispersion X-ray spectroscopy (EDS; EDAX X-ray analyzer). The composition and binding energies of the nanorods were investigated with a Kratos Axis Ultra XPS system containing a DLD detector. A Shirley background correction was applied to all XPS spectra, and the binding energy was calibrated to Ag $3d_{5/2}$ = 368.4 eV. Photonic properties of our nanostructures were characterized using bright field illumination with linearly polarized light on a Zeiss Axio Imager M1m optical microscope. Samples were dispersed on glass microscope slides. Scattered light from the nanostructures was collected with a 150 × objective and analyzed using a PI Acton MicroSpec-2360 spectrometer with a PIXIS 400BR CCD camera system.

Acknowledgment. This research was supported in part by the Natural Sciences and Engineering Research Council (NSERC) of Canada, the Canada Research Chairs Program, and Simon Fraser University (Trust Endowment Fund). This work made use of 4D LABS shared facilities and infrastructure in Gates' laboratory supported by the Canada Foundation for Innovation (CFI), British Columbia Knowledge Development Fund (BCKDF), and Simon Fraser University. We also gratefully acknowledge the assistance of Michael C. P. Wang in the process of collecting and fitting the XPS data.

Supporting Information Available: Photograph of our setup for electrodeposition of silver, SEM images of the polymer mold before and after filling with electrodeposited silver, SEM images for the overfilling of the polymer mold with deposited silver, SEM images of unetched porous nanorods, and XPS analysis of the nanorods. This material is available free of charge *via* the Internet at http://pubs.acs.org.

REFERENCES AND NOTES

1. Zhang, L.; Gu, F. X.; Chan, J. M.; Wang, A. Z.; Langer, R. S.; Farokhzad, O. C. nanoparticles in Medicine: Therapeutic Applications and Developments. *Clin. Pharmacol. Ther.* **2008**, *83*, 761–769.
2. Roy, I.; Ohulchanskyy, T. Y.; Pudavar, H. E.; Bergey, E. J.; Oseroff, A. R.; Morgan, J.; Dougherty, T. J.; Prasad, P. N. Ceramic-Based nanoparticles Entrapping Water-Insoluble Photosensitizing Anticancer Drugs: A Novel Drug-Carrier System for Photodynamic Therapy. *J. Am. Chem. Soc.* **2003**, *125*, 7860–7865.
3. Chithrani, B. D.; Ghazani, A. A.; Chan, W. C. W. Determining the Size and Shape Dependence of Gold nanoparticle Uptake into Mammalian Cells. *nano Lett.* **2006**, *6*, 662–668.
4. Gao, X.; Tao, W.; Lu, W.; Zhang, Q.; Zhang, Y.; Jiang, X.; Fu, S. Lectin-Conjugated PEG-PLA nanoparticles: Preparation and Brain Delivery after Intranasal Administration. *Biomaterials* **2006**, *27*, 3482–3490.
5. Pérez-Juste, J.; Pastoriza-Santos, I.; Liz-Marzán, L. M.; Mulvaney, P. Gold nanorods: Synthesis, Characterization and Applications. *Coord. Chem. Rev.* **2005**, *249*, 1870–1901.
6. Scholes, G. D. Controlling the Optical Properties of Inorganic nanoparticles. *Adv. Funct. Mater.* **2008**, *18*, 1157–1172.
7. Sando, G. M.; Berry, A. D.; Campbell, P. M.; Baronavski, A. P.; Owrutsky, J. C. Surface Plasmon Dynamics of High-Aspect-Ratio Gold nanorods. *Plasmonics* **2007**, *2*, 23–29.
8. Medintz, I. L.; Uyeda, H. T.; Goldman, E. R.; Mattoussi, H. Quantum Dot Bioconjugates for Imaging, Labeling and Sensing. *Nat. Mater.* **2005**, *4*, 435–446.
9. Larson, D. R.; Zipfel, W. R.; Williams, R. M.; Clark, S. W.; Bruchez, M. P.; Wise, F. W.; Webb, W. W. Water-Soluble Quantum Dots for Multiphoton Fluorescence Imaging *In Vivo*. *Science* **2003**, *300*, 1434–1436.
10. Chan, W. C. W.; Nie, S. Quantum Dot Bioconjugates for Ultrasensitive Nonisotopic Detection. *Science* **1998**, *281*, 2016–2018.

11. Bruchez, M., Jr.; Morronne, M.; Gin, P.; Weiss, S.; Alivisatos, A. P. Semiconductor nanocrystals as Fluorescent Biological Labels. *Science* **1998**, *281*, 2013–2016.
12. Ji, C.; Searson, P. C. Fabrication of nanoporous Gold nanowires. *Appl. Phys. Lett.* **2002**, *81*, 4437–4439.
13. Laocharoensuk, R.; Sattayasamitsathit, S.; Burdick, J.; Kanatharana, P.; Thavarungkul, P.; Wang, J. Shape-Tailored Porous Gold nanowires: From nano Barbells to nano Step-Cones. *ACS nano* **2007**, *1*, 403–408.
14. Hunyadi, S. E.; Murphy, C. J. Bimetallic Silver−Gold nanowires: Fabrication and Use in Surface-Enhanced Raman Scattering. *J. Mater. Chem.* **2006**, *16*, 3929–3935.
15. Sun, Y.; Xia, Y. Mechanistic Study on the Replacement Reaction between Silver nanostructures and Chloroauric Acid in Aqueous Medium. *J. Am. Chem. Soc.* **2004**, *126*, 3892–3901.
16. Skrabalak, S. E.; Chen, J.; Au, L.; Lu, X.; Li, X.; Xia, Y. Gold nanocages for Biomedical Applications. *Adv. Mater.* **2007**, *19*, 3177–3184.
17. Hulteen, J. C.; Martin, C. R. A General Template-Based Method for the Preparation of nanomaterials. *J. Mater. Chem.* **1997**, *7*, 1075–1087.
18. Sauer, G.; Brehm, G.; Schneider, S.; Nielsch, K.; Wehrspohn, R. B.; Choi, J.; Hofmeister, H.; Gösele, U. Highly Ordered Monocrystalline Silver nanowire Arrays. *J. Appl. Phys.* **2002**, *91*, 3243–3247.
19. Barbic, M.; Mock, J. J.; Smith, D. R.; Schultz, S. Single Crystal Silver nanowires Prepared by the Metal Amplification Method. *J. Appl. Phys.* **2002**, *91*, 9341–9345.
20. Kazeminezhad, I.; Barnes, A. C.; Holbrey, J. D.; Seddon, K. R.; Schwarzacher, W. Templated Electrodeposition of Silver nanowires in a nanoporous Polycarbonate Membrane from a Nonaqueous Ionic Liquid Electrolyte. *Appl. Phys. A: Mater. Sci. Process.* **2007**, *86*, 373–375.
21. Figure S2 in Supporting Information contains images showing the percentage of pores that have been filled with silver nanorods.
22. See Figure S3 in Supporting Information for an SEM image of a membrane after the pores have been overfilled.
23. Pomfret, M. B.; Brown, D. J.; Epshteyn, A.; Purdy, A. P.; Owrutsky, J. C. Electrochemical Template Deposition of Aluminum nanorods Using Ionic Liquids. *Chem. Mater.* **2008**, *20*, 5945–5947.
24. Schönenberger, C.; van der Zande, B. M. I.; Fokkink, L. G. J.; Henny, M.; Schmid, C.; Krüger, M.; Bachtold, A.; Huber, R.; Birk, H.; Staufer, U. Template Synthesis of nanowires in Porous Polycarbonate Membranes: Electrochemistry and Morphology. *J. Phys. Chem. B* **1997**, *101*, 5497–5505.
25. Chen, C.; Wang, L.; Jiang, G.; Zhou, J.; Chen, X.; Yu, H.; Yang, Q. Study on the Synthesis of Silver nanowires with Adjustable Diameters through the Polyol Process. *nanotechnology* **2006**, *17*, 3933–3938.
26. Sun, Y.; Mayer, B.; Herricks, T.; Xia, Y. Polyol Synthesis of Uniform Silver nanowires: A Plausible Growth Mechanism and the Supporting Evidence. *nano Lett.* **2003**, *3*, 955–960.
27. Busbee, B. D.; Obare, S. O.; Murphy, C. J. An Improved Synthesis of High-Aspect-Ratio Gold nanorods. *Adv. Mater.* **2003**, *15*, 414–416.
28. Majidi, E.; Gates, B. D. Optimizing Growth Rates and Thermal Stability of Silver nanowires. *Mater. Res. Soc. Symp. Proc.* **2007**, *1017*, 1017-DD18-12.
29. Tian, N.; Zhou, Z.-Y.; Sun, S.-G.; Wang, Z. L. Synthesis of Tetrahexahedral Platinum nanocrystals with High-Index Facets and High Electro-Oxidation Activity. *Science* **2007**, *316*, 732–735.
30. Somorjai, G. A.; Blakely, D. W. Mechanism of Catalysis of Hydrocarbon Reactions by Platinum Surfaces. *Nature* **1975**, *258*, 580–583.
31. Figure S4 in the Supporting Information contains images of the nanorods before the excess silver has been removed with ammonium hydroxide.
32. Figure S5 in the Supporting Information contains XPS spectra and peak positions corresponding to the analysis of Au and Ag within the hollow nanorods.
33. Liu, Y.-C.; Lee, H.-T.; Peng, H.-H. New Pathway for Sonoelectrochemical Synthesis of Gold−Silver Alloy nanoparticles from Their Bulk Substrates. *Chem. Phys. Lett.* **2004**, *400*, 436–440.
34. Jain, P. K.; Lee, K. S.; El-Sayed, I. H.; El-Sayed, M. A. Calculated Absorption and Scattering Properties of Gold nanoparticles of Different Size, Shape, and Composition: Applications in Biological Imaging and Biomedicine. *J. Phys. Chem. B* **2006**, *110*, 7238–7248.
35. Mock, J. J.; Oldenburg, S. J.; Smith, D. R.; Schultz, D. A.; Schultz, S. Composite Plasmon Resonant nanowires. *nano Lett.* **2002**, *2*, 465–469.
36. Willets, K. A.; Van Duyne, R. P. Localized Surface Plasmon Resonance Spectroscopy and Sensing. *Annu. Rev. Phys. Chem.* **2007**, *58*, 267–297.
37. Malinsky, M. D.; Kelly, K. L.; Schatz, G. C.; Van Duyne, R. P. Chain Length Dependence and Sensing Capabilities of the Localized Surface Plasmon Resonance of Silver nanoparticles Chemically Modified with Alkanethiol Self-Assembled Monolayers. *J. Am. Chem. Soc.* **2001**, *123*, 1471–1482.
38. Daniel, M.-C.; Astruc, D. Gold nanoparticles: Assembly, Supramolecular Chemistry, Quantum-Size-Related Properties, and Applications toward Biology, Catalysis, and nanotechnology. *Chem. Rev.* **2004**, *104*, 293–346.
39. Love, J. C.; Estroff, L. A.; Kriebel, J. K.; Nuzzo, R. G.; Whitesides, G. M. Self-Assembled Monolayers of Thiolates on Metals as a Form of nanotechnology. *Chem. Rev.* **2005**, *105*, 1103–1169.
40. Ulman, A. Formation and Structure of Self-Assembled Monolayers. *Chem. Rev.* **1996**, *96*, 1533–1554.
41. Bourg, M.-C.; Badia, A.; Lennox, R. B. Gold−Sulfur Bonding in 2D and 3D Self-Assembled Monolayers: XPS Characterization. *J. Phys. Chem. B* **2000**, *104*, 6562–6567.
42. Chen, J.; Wang, D.; Xi, J.; Au, L.; Siekkinen, A.; Warsen, A.; Li, Z.-Y.; Zhang, H.; Xia, Y.; Li, X. Immuno Gold nanocages with Tailored Optical Properties for Targeted Photothermal Destruction of Cancer Cells. *nano. Lett.* **2007**, *7*, 1318–1322.
43. Huang, X.; El-Sayed, I. H.; Qian, W.; El-Sayed, M. A. Cancer Cell Imaging and Photothermal Therapy in the Near-Infrared Region by Using Gold nanorods. *J. Am. Chem. Soc.* **2006**, *128*, 2115–2120.
44. Menon, V. P.; Martin, C. R. Fabrication and Evaluation of nanoelectrode Ensembles. *Anal. Chem.* **1995**, *67*, 1920–1928.